

Analysis of the expected resolution of the electron-cyclotron emission crossed-sightline magnetic field diagnostic

G. R. Hanson and C. E. Thomas Jr.

Citation: [Review of Scientific Instruments](#) **61**, 671 (1990); doi: 10.1063/1.1141478

View online: <http://dx.doi.org/10.1063/1.1141478>

View Table of Contents: <http://scitation.aip.org/content/aip/journal/rsi/61/2?ver=pdfcov>

Published by the [AIP Publishing](#)

Articles you may be interested in

[Electron-cyclotron damping of helicon waves in low diverging magnetic fields](#)

Phys. Plasmas **18**, 043502 (2011); 10.1063/1.3573864

[Crossed-sightline correlation of thermal ECE for remote measurement of absolute magnetic fields \(abstract\)](#)

Rev. Sci. Instrum. **63**, 4636 (1992); 10.1063/1.1143641

[Autocorrelation and crossed-sightline correlation of ECE for measurement of electron temperature and density fluctuations on ATF and TEXT](#)


Rev. Sci. Instrum. **61**, 3570 (1990); 10.1063/1.1141573

[Autocorrelation and crossed-sightline correlation of ECE for measurement of electron temperature and density fluctuations on ATF and TEXT \(abstract\)](#)

Rev. Sci. Instrum. **61**, 3073 (1990); 10.1063/1.1141737

[Electron-cyclotron resonance heating in plasmas with arbitrary stratification of the magnetic field](#)

Phys. Fluids **24**, 1097 (1981); 10.1063/1.863489

The advertisement for Mad City Labs Inc. (MCL) features the company logo at the top center, which consists of the letters 'MCL' in a large, red, stylized font, with 'MAD CITY LABS INC.' in a smaller, red, sans-serif font below it. Below the logo, there are four images of different products, each with a label underneath. From left to right: 1. A white, square-shaped device with a central square cutout, labeled 'Nanopositioning Systems'. 2. A small, black, rectangular device, labeled 'Micropositioning'. 3. A device with a yellow and black striped pattern, labeled 'AFM & SPM'. 4. A larger, black, rectangular device with a small, black, rectangular component attached to its side, labeled 'Single molecule imaging'.

Analysis of the expected resolution of the electron-cyclotron emission crossed-sightline magnetic field diagnostic

G. R. Hanson and C. E. Thomas, Jr.

Nuclear Engineering Program, Georgia Institute of Technology, Atlanta, Georgia 30332

(Received 13 March 1989; accepted for publication 6 October 1989)

The local value of the magnetic field $B(r)$ inside the plasma in magnetic fusion experiments is a quantity of considerable interest. Given information about plasma density and temperature it can be used to calculate the poloidal magnetic field, or given a zero current device (or the current profile) the local value of beta. The time history $B(r, t)$ can be used to infer the level of magnetic fluctuations in the plasma. The poloidal magnetic field and the level of magnetic fluctuations are particularly interesting quantities, since they are difficult to measure, and are both important for understanding particle and energy transport in magnetic fusion experiments. In fact, to date, no measurement of the local value of the total magnetic field or its time variation has been made in a high temperature plasma. Previous measurements have been confined to relatively cold plasmas where probes could be used, or have inadequate resolution to distinguish the value of the field with plasma present from its vacuum value. It has been recently suggested that crossed-sightline correlation of electron-cyclotron emission might be used to infer $B(r_x, t)$ at the crossing point r_x in the plasma of the two sightlines. The equations and techniques necessary to simulate this proposed diagnostic are developed below, and the results of a numerical simulation of the diagnostic resolution for both TEXT and CIT are presented.

I. INTRODUCTION

It has been suggested that crossed-sightline correlation of electron cyclotron emission (ECE) might be used to experimentally measure the absolute value of the local magnetic field and its time variation in a tokamak plasma.¹ The basic idea is to time correlate the ECE received by two antennas having sightlines which cross in the plasma (see Fig. 1) to obtain the cross-correlation function. This function will represent the ECE near the crossing volume of the two sightlines (for short correlation lengths). By resolving the line center (in frequency space) of this correlated emission and following it in time (at frequencies less than $1/T$, where T is the correlation time), the total magnetic field $B(t)$ can be measured since the local value of the cyclotron frequency ω_b is given by

$$\omega_b = qB(t)/m_e, \quad (1)$$

where q is the electron charge, and m_e is the electron mass. References 1 and 2 provide a more detailed discussion of the theory and conceptual design of this diagnostic.

The sightlines can be scanned so that a magnetic field profile over a portion of the minor radius can be constructed. If the density and temperature are known, then the poloidal magnetic field can be calculated over this region. In zero current devices, the measurement is a direct measurement of β , or if the current profile is known or estimated, β can be calculated. If multiple sightlines are used, then a magnetic field profile, and therefore poloidal field or β profiles, across the minor radius can be constructed without scanning.

We have developed a numerical routine which simulates the correlated signal from the crossed-sightline diagnostic and then determines the error in the magnetic field inferred from the simulated data. To obtain this simulated data, the

uncertainties in the cross-correlation function are estimated and then used by a Monte Carlo routine to randomize the expected cross-correlation function. A nonlinear curve-fitting routine³ is used to fit a function to the randomized data so that the error in the line center due to the expected experimental errors can be calculated.

This numerical routine has been used to perform magnetic fluctuation and absolute magnetic field strength $|B|$ measurement simulations for TEXT (Texas Tokamak, University of Texas at Austin) and CIT (the proposed Compact Ignition Tokamak). We believe the results of these simulations show that the proposed diagnostic will be able to measure perpendicular magnetic fluctuations with an error of the order of 4% of the toroidal magnetic field and measure the absolute magnetic field strength with an error of the order of 0.1%. The error in measurement of parallel magnetic fluctuations will also be about 0.1% of the toroidal magnetic field, the same order as the error in the absolute magnetic field. This will be discussed further in Sec. IV B.

A second numerical simulation has been developed to determine the uncertainty in inferring the poloidal magnetic field from the $|B|$ measurement. In this simulation, the uncertainty in the poloidal magnetic field is calculated from the contributing field terms and their uncertainties. Results of this simulation indicate that the poloidal magnetic field can be inferred from the $|B|$ measurement for $r/a > 0.2$ with an uncertainty of less than 10.0% under many conditions. Inferring the poloidal magnetic field from the $|B|$ measurement is discussed in more detail in Sec. IV C.

II. CORRELATION FUNCTIONS

Figures 1 and 2 show the conceptual design of the diagnostic.² The design of a single sightline in this diagnostic is

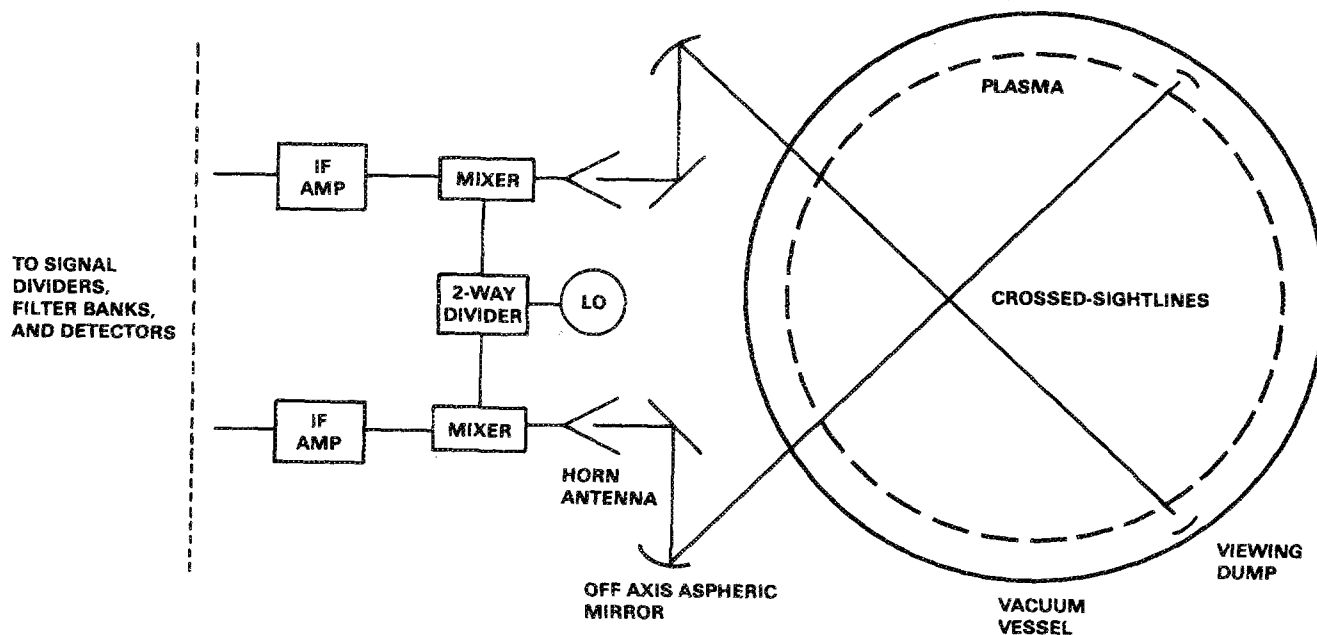


FIG. 1. Conceptual schematic of the antenna system, viewing sightlines and dumps, and mixer, local oscillator (LO), and intermediate frequency (IF) amplifier for crossed-sightline system.

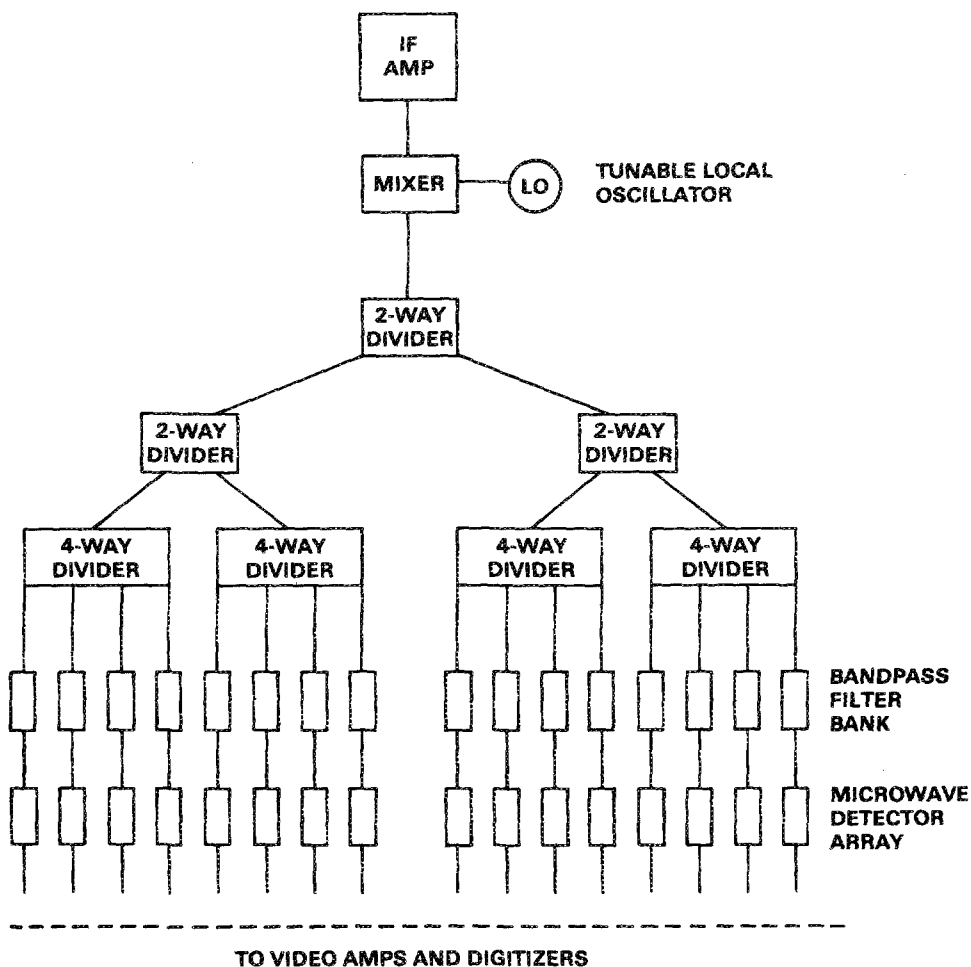


FIG. 2. Conceptual schematic of the balance of the microwave electronics for the crossed-sightline ECE system (see Fig. 1 for the front end).

very similar to the design of the ECE diagnostic on ATF.⁴ The received signal at each antenna will be bandpass filtered into passbands $\delta\omega_i$ about frequency ω_i at time t and fed into microwave detectors. Let the signals out of these detectors due to emission along each sightline be described by $I_1(\omega_i, t)$ and $I_2(\omega_i, t)$ for antennas 1 and 2, respectively, where ω_i is the center frequency of the i th channel of the detector array. For a turbulent plasma, signals I_1 and I_2 will have a steady-state part \bar{I}_1, \bar{I}_2 and a fluctuating part i_1, i_2 , in which case

$$I_1(\omega_i, t) = \bar{I}_1(\omega_i) + i_1(\omega_i, t) \quad (2)$$

and

$$I_2(\omega_i, t) = \bar{I}_2(\omega_i) + i_2(\omega_i, t). \quad (3)$$

The steady-state parts of I_1 and I_2 are given by their mean values,

$$\bar{I}_1(\omega_i) = \frac{1}{T} \int_0^T I_1(\omega_i, t) dt \quad (4)$$

and

$$\bar{I}_2(\omega_i) = \frac{1}{T} \int_0^T I_2(\omega_i, t) dt, \quad (5)$$

where T is the averaging time. Note that I_1 and I_2 can be electronically high-pass filtered to remove \bar{I}_1 and \bar{I}_2 , or this can be done in software.

The equal time correlation function is defined as⁵

$$R_{lk} = \lim_{T \rightarrow \infty} \frac{1}{T} \int_0^T i_l(t) i_k(t) dt, \quad (6)$$

where R_{lk} is precisely the cross-correlation function if i_l and i_k have mean values of zero, and again T is the averaging or correlation time. The autocorrelation function is defined as the special case when $l = k$. For the crossed sightlines of this diagnostic, the equal time cross-correlation function is estimated by

$$R_{12}(\omega_i, t) = \frac{1}{T} \int_{-T/2}^{T/2} i_1(\omega_i, t + \tau) i_2(\omega_i, t + \tau) d\tau \\ = \langle i_1(\omega_i, t) i_2(\omega_i, t) \rangle, \quad (7)$$

where $\langle \rangle$ is defined as the equal time correlation function operator, and T is a finite period.

If j_1 and j_2 are defined as the local values of the fluctuating part of the emission at positions s_1 and s_2 along the two sightlines; that is,

$$j_1(\omega_i, s_1, t) = di_1/ds_1 \quad (8)$$

and

$$j_2(\omega_i, s_2, t) = di_2/ds_2, \quad (9)$$

where s_1 and s_2 represent respective positions on the two sightlines, then Eq. (7) can be written as

$$R_{12}(\omega_i, t) = \left\langle \int ds_1 \int ds_2 j_1(\omega_i, s_1, t) j_2(\omega_i, s_2, t) \right\rangle. \quad (10)$$

By definition, in regions of a turbulent plasma that are separated by more than a correlation length l_c , the time-correlation (cross-correlation) function rapidly goes to zero, in which case R_{12} can be written as

$$R_{12}(\omega_i, t) = \int_{r_x - l_c}^{r_x + l_c} ds_1 \int_{r_x - l_c}^{r_x + l_c} ds_2 \\ \times \langle j_1(\omega_i, s_1, t) j_2(\omega_i, s_2, t) \rangle, \quad (11)$$

where r_x is the spatial crossing point of the two sightlines, and the time operator has been passed through the two spatial integrals. It can be seen from the above equation that as the correlation length becomes small, the cross-correlation of j_1 and j_2 comes only from the crossing volume of the two antenna sightlines.

III. UNCERTAINTY IN THE CROSS-CORRELATION FUNCTION

The variance of the cross-correlation function of i_1 and i_2 for identical bandwidths, Δf , is⁵

$$\sigma_{12}^2 = (R_{11}R_{22} + R_{12}^2)/(2\Delta f T), \quad (12)$$

where T is the correlation time of i_1 and i_2 in Eq. (7), σ_{12} is the variance, Δf is the effective bandwidth, and $R_{ij}(\omega_i, t)$ has been previously defined. For convenience we will often shorten $R_{ij}(\omega_i, t)$ to R_{ij} . The requirement that $\Delta f T \gg 5$ is used in obtaining this equation.

The uncertainty in $R_{12}(\omega_i, t)$ is estimated from (also from Ref. 5)

$$\epsilon^2 \equiv \sigma_{12}^2 / R_{12}^2 = (1 + \rho_{12}^2)/(2\Delta f T), \quad (13)$$

where

$$\rho_{12} = R_{12} / \sqrt{R_{11}R_{22}} \quad (14)$$

is the cross-correlation coefficient. Equation (13) can be rewritten as

$$\sigma_{12} = R_{12}(\omega_i, t) [(1 + \rho_{12}^2)/N]^{1/2}, \quad (15)$$

where N is the number of data points used in calculating $R_{12}(\omega_i, t)$ [see Bendat and Piersol⁵ for the derivation of Eq. (15)].

The signals i_1 and i_2 can be written as

$$i_1(\omega, t) = s(\omega, t) + m(\omega, t) \quad (16)$$

and

$$i_2(\omega, t) = s(\omega, t) + n(\omega, t), \quad (17)$$

where $s(\omega, t)$ is the correlated emission, and $m(\omega, t)$ and $n(\omega, t)$ are uncorrelated emission (noise for our purposes). If it is assumed that $s(\omega, t)$, $m(\omega, t)$, and $n(\omega, t)$ are mutually uncorrelated, then the cross and auto-correlation functions can be written as

$$R_{12} = R_{ss} \equiv \langle s^2 \rangle, \quad (18)$$

$$R_{11} = R_{ss} + R_{mm} \equiv \langle s^2 \rangle + \langle m^2 \rangle, \quad (19)$$

$$R_{22} = R_{ss} + R_{nn} \equiv \langle s^2 \rangle + \langle n^2 \rangle, \quad (20)$$

where

$$\langle s^2 \rangle = \frac{1}{T} \int_{-T/2}^{T/2} s^2(\omega, t + \tau) d\tau, \quad (21)$$

$$\langle m^2 \rangle = \frac{1}{T} \int_{-T/2}^{T/2} m^2(\omega, t + \tau) d\tau, \quad (22)$$

$$\langle n^2 \rangle = \frac{1}{T} \int_{-T/2}^{T/2} n^2(\omega, t + \tau) d\tau. \quad (23)$$

For this diagnostic where the two crossed sightlines are ar-

ranged symmetrically about the tokamak midplane, $\langle m^2 \rangle$ and $\langle n^2 \rangle$ are probably due to equivalent physical phenomena. In this case, they can be treated as equivalent but uncorrelated noise sources, i.e., $\langle n^2 \rangle = \langle m^2 \rangle$. Substituting these relations into the equation for the cross-correlation coefficient produces the desired result,

$$\rho_{12} = 1/(1 + \langle n^2 \rangle / \langle s^2 \rangle). \quad (24)$$

IV. POSSIBLE MEASUREMENTS

A. Overview

The cross-correlation function R_{12} can be used to infer several different plasma parameters. From the center frequency of $R_{12}(\omega, t)$, the absolute magnetic field strength $|\mathbf{B}|$ at the crossing volume of the two sightlines can be calculated, and from $|\mathbf{B}|$, the poloidal magnetic field can be inferred. By following the peak of $R_{12}(\omega, t)$ in frequency space, fluctuations in $|\mathbf{B}|$ can be measured. The correlation length for fluctuations at the crossing volume can be inferred from the width in frequency space of $R_{12}(\omega, t)$. Finally, at optically thick harmonics, temperature fluctuations can be inferred from the amplitude of R_{12} , or at optically thin harmonics a summation of temperature and density fluctuations can be obtained. This assumes that magnetic fluctuations are small compared to temperature and density fluctuations. Below we discuss only magnetic fluctuation measurements, and poloidal magnetic field measurements inferred from $|\mathbf{B}|$.

B. Magnetic fluctuations

Consider the following equation for $|\mathbf{B}|$ (Ref. 6):

$$|\mathbf{B}| = (\mathbf{B} \cdot \mathbf{B})^{1/2}. \quad (25)$$

Using $\mathbf{B} = \mathbf{B}_0 + \tilde{\mathbf{B}}_\perp + \tilde{\mathbf{B}}_\parallel$ in the above equation, where \mathbf{B}_0 is the magnetic field including the plasma current and diamagnetic contributions, and $\tilde{\mathbf{B}}_\perp$ and $\tilde{\mathbf{B}}_\parallel$ are the fluctuations perpendicular and parallel to \mathbf{B}_0 , gives

$$|\mathbf{B}| = (B_0^2 + 2\tilde{\mathbf{B}}_\perp \cdot \mathbf{B}_0 + \tilde{\mathbf{B}}_\perp^2 + \tilde{\mathbf{B}}_\parallel^2)^{1/2}. \quad (26)$$

Now factoring out B_0 and expanding the expression (for $\tilde{\mathbf{B}}_\perp$ and $\tilde{\mathbf{B}}_\parallel$ much less than \mathbf{B}_0) leads to

$$|\mathbf{B}| = B_0 [1 + (\tilde{\mathbf{B}}_\parallel / B_0) + 1/2(\tilde{\mathbf{B}}_\perp / B_0)^2], \quad (27)$$

where only the lowest order terms in $\tilde{\mathbf{B}}_\parallel$ and $\tilde{\mathbf{B}}_\perp$ have been retained. Examining the last equation leads to the conclusion that parallel fluctuations in \mathbf{B}_0 are reflected linearly as fluctuations in $|\mathbf{B}|$, but that small perpendicular fluctuations are down by $1/2(\tilde{\mathbf{B}}_\perp / B_0)$ from the linear response. For instance, for a 1% perpendicular fluctuation, the change in $|\mathbf{B}|$ would be only 0.005%. This is unfortunate since it is thought that the magnetic fluctuations which might lead to enhanced transport will be perpendicular. Nevertheless, the diagnostic will have the capability of measuring any parallel fluctuations with the same resolution as its resolution in $|\mathbf{B}|$, and will be able to infer the correlation length of fluctuations in the plasma.

C. Poloidal magnetic field

Again consider Eq. (25) for $|\mathbf{B}|$, but now use $\mathbf{B} = \mathbf{B}_v + \mathbf{B}_p + \mathbf{B}_d$, where \mathbf{B}_v is the toroidal vacuum field,

\mathbf{B}_p is the field due to the force-free plasma currents, and \mathbf{B}_d is the plasma diamagnetic contribution. Then $|\mathbf{B}|$ can be written as

$$|\mathbf{B}| = (B_v^2 + B_p^2 + B_\theta^2 + B_d^2 + 2B_v B_{\phi p} - 2B_v B_d - 2B_{\phi p} B_d)^{1/2},$$

where $B_{\phi p}$ and B_θ are the toroidal and poloidal fields, respectively, produced by the force-free plasma current. This equation reduces to

$$|\mathbf{B}| = [B_v^2(1 - \beta) + B_{\phi p}^2 + B_\theta^2 + 2B_v B_{\phi p}(1 - \beta/2)]^{1/2} \quad (29)$$

by using the toroidal equilibrium equation:

$$B_v^2/2\mu_0 = B_i^2/2\mu_0 + p, \quad (30)$$

with $B_i^2 = \mathbf{B}_i \cdot \mathbf{B}_i$ and $\mathbf{B}_i = \mathbf{B}_v + \mathbf{B}_d$ to define B_d . The equation for β ,

$$\beta = p/(B_v^2/2\mu_0) \quad (31)$$

is used to eliminate the plasma pressure p from Eq. (30).

Equation (29) can then be solved to obtain an expression for B_θ^2 ,

$$B_\theta^2 = [|\mathbf{B}|^2 - B_v^2(1 - \beta) - B_{\phi p}^2 - 2B_v B_{\phi p}(1 - \beta/2)]. \quad (32)$$

Since $|\mathbf{B}|$ is known from the diagnostic measurements, B_v is known from field measurements, β is obtainable from other diagnostics, and $B_{\phi p}$ can be estimated or calculated using an MHD equilibrium code, the value of B_θ at the sightline crossing point can be determined.

V. NUMERICAL SIMULATION OF $|\mathbf{B}|$ MEASUREMENT

A. Overview

The purpose of simulating the data is to investigate the potential error in the measurement, and under what conditions this error becomes too large for magnetic field measurements to be possible. Time varying magnetic field measurements are made by following the line center of the ECE correlation function $R_{12}(\omega_i, t)$ plotted versus frequency as it fluctuates in time. Thus to make a magnetic field measurement, we must know the center frequency of the correlation function $R_{12}(\omega_i, t)$ very accurately relative to its width.

Our numerical simulation assumes that $R_{12}(\omega_i, t)$ has a Gaussian line shape in frequency (ω_i) space. The specified plasma and diagnostic conditions are used to calculate the width $\delta\omega_c$ in frequency space of $R_{12}(\omega_i, t)$. In addition the uncertainty σ_{12i} at each ω_i of $R_{12}(\omega_i, t)$ is calculated. The projected uncertainty σ_{12i} in each point $R_{12}(\omega_i, t)$ is used in a Monte Carlo routine to randomize the calculated values of $R_{12}(\omega_i, t)$. This simulates the expected experimental variation in $R_{12}(\omega_i, t)$. A nonlinear curve-fitting routine then fits a Gaussian distribution to the randomized data and determines the line center. This is repeated for many sets of randomized data. The standard deviation is then obtained from the set of calculated means and the actual line center (true mean). For plotting purposes, we have divided the standard deviation by the true line center to obtain the expected fractional error in the experimental line center.

B. Expected line shape

The expected line shape of the cross-correlation function $R_{12}(\omega_i, t)$ versus frequency ω_i is difficult to calculate as it depends on the natural spatial line width (l_{ns}) of the ECE, the correlation length (l_c) and correlation function shape in the plasma, the crossing length of the two antenna sightlines (l_x), and the wavelength of the magnetic fluctuation being measured (for magnetic fluctuation measurements). It is quite probable that the cross-correlation function will have a Gaussian distribution. This statement is supported by the *central limit theorem*,⁵ which asserts that the Gaussian distribution will result quite generally from the sum of a large number of independent random variables acting together. Assuming the turbulent modes in the plasma are independent, the Gaussian shape follows.

For the numerical simulation, it is assumed that the crossed sightlines will be arranged perpendicular to the magnetic field so that the natural linewidth will be due to relativistic broadening of the emission. In general, the requirement of perpendicularity is relaxed to requiring that the Doppler broadening be less than the relativistic broadening. This allows for some deviation from true perpendicularity of the sightlines to the magnetic field. The natural linewidth $\delta\omega_n$ (full width at half maximum) due to relativistic broadening is given by⁷

$$\delta\omega_n/s\omega_b = c_s(v_{te}/c)^2, \quad (33)$$

where ω_b is the fundamental cyclotron frequency, and v_{te} is the electron thermal velocity [but is defined as $v_{te} = (T/m)^{1/2}$ rather than the more standard $(2T/m)^{1/2}$]. Here s is the harmonic number, and c_s is a constant which changes with harmonic number, e.g., for $s = 3$, $c_s = 4.8$.

To calculate the variance in frequency space of $R_{12}(\omega_i, t)$, it is assumed that the two dominant factors are the correlation length and the natural linewidth. If the natural ECE linewidth in frequency space is considered as its equivalent spatial linewidth,

$$l_{ns} = \frac{B}{\nabla B} \frac{\delta\omega_n}{s\omega_b} = Rc_s \left(\frac{v_{te}}{c} \right)^2, \quad (34)$$

then the variance is approximated by

$$\delta\omega_c^2 = (\omega_0^2/R^2)(l_c^2 + l_{ns}^2), \quad (35)$$

where $\delta\omega_c$ is the width in frequency space of the cross-correlation function $R_{12}(\omega_i, t)$, ω_0 is the cyclotron harmonic frequency under consideration at the crossing point of the two sightlines [line center of $R_{12}(\omega_i, t)$], and R is the tokamak major radius at the crossing point of the two sightlines. Note that this defines the correlation function in frequency space,

$$R_{12}(\omega_i, t) = R_{12}(\omega_0) \exp \left\{ -\frac{1}{2} [(\omega_i - \omega_0)/\delta\omega_c]^2 \right\}, \quad (36)$$

where ω_i is the center frequency of the i th channel, and the time dependence of ω_0 has been suppressed. Once $\delta\omega_c$ and ω_0 are calculated, a continuous Gaussian distribution for $R_{12}(\omega_i, t)$ is defined.

C. Estimating the correlation noise

The next step in the simulation is to estimate the uncertainty in each value of $R_{12}(\omega_i, t)$ using Eq. (15),

$$\sigma_{12i} = R_{12}(\omega_i, t) [(1 + \rho_{12i}^{-2})/N]^{1/2}, \quad (37)$$

where the subscript i indicates that σ_{12} is calculated at the center frequency of the i th channel.

The cross-correlation coefficient ρ_{12i} is calculated using Eq. (24). To do this, we must estimate the sources of the noise $\langle n^2 \rangle$. The uncorrelated signal (noise) can be divided into two categories: noise produced in the plasma and noise produced in the microwave hardware. If we approximate the hardware noise as 1 eV black body emission,⁸ our ECE power calculations for TEXT show the hardware noise to be down by at least two orders of magnitude relative to the signal, and we find that plasma noise dominates.

The remaining noise can be divided into three sources: the quantum or photon noise at the detectors, the uncorrelated signal incident on the antenna due to reflections off the vacuum vessel, and uncorrelated emission along the sightline.

Radiometer theory⁹ has shown that for thermal emission, the statistical fluctuation about the average signal value is given by

$$n_q = S_T / \sqrt{\tau \delta\omega_i / 2\pi}, \quad (38)$$

where n_q is the quantum noise, S_T is the total average received signal, $\delta\omega_i$ is the bandwidth of the channel (previously defined), and τ is the microwave crystal detector integration time. It is assumed that the statistical fluctuations are incoherent. The Appendix discusses the possible coherence of the statistical fluctuations of thermal cyclotron emission and the effect of this coherence on a crossed sightline diagnostic. The total average received signal is defined as the dc signal plus vacuum vessel reflections. This can be written as

$$S_T = \bar{I} + Q\bar{I}(1 - \eta), \quad (39)$$

where \bar{I} is as before, Q is the cavity resonance term for the vacuum vessel, and η is the viewing dump efficiency (absorption coefficient). The vacuum vessel cavity resonance is defined as

$$Q = 1/(1 - R_w), \quad (40)$$

where R_w is the wall reflectivity of the vacuum vessel.

To calculate the correlation coefficient ρ_{12i} , the noise terms must be normalized to the correlated signal $s(\omega_i, t)$ [see Eq. (24)]. Thus the normalized quantum noise can be written as

$$\frac{n_q}{s(\omega_i, t)} = \frac{1 + Q(1 - \eta)}{A_f \sqrt{\tau \delta\omega_i / 2\pi}}, \quad (41)$$

where A_f is the emission fluctuation fraction due to correlated fluctuations in density, temperature, or magnetic field and is defined as

$$\begin{aligned} A_f &\equiv s(\omega_i, t) / \bar{I} \\ &\approx \frac{1}{\bar{I}} \left\{ R_{12}(\omega_0) \exp \left[-\frac{1}{2} \left(\frac{\omega_i - \omega_0}{\delta\omega_c} \right)^2 \right] \right\}^{1/2} \\ &= A_{f0} \exp \left\{ -\frac{1}{4} [(\omega_i - \omega_0)/\delta\omega_c]^2 \right\}, \end{aligned} \quad (42)$$

and A_{f0} is defined as the emission fluctuation fraction at the line center ω_0 . The second equality above follows by using Eq. (36) in Eq. (21) and approximating $s^2(t) \approx \langle s^2 \rangle$.

Radiation at the same frequency as the line center of the correlation function will be emitted at many points in the plasma besides the crossing volume. This radiation must be prevented from being collected by the diagnostic system. The beamlike pattern of the antenna will allow only emission along the sightline to be collected; however, radiation can be reflected from the vacuum vessel into the antenna sightline. This reflection noise is minimized by using a viewing dump to absorb the incident radiation. Due to incomplete absorption by the viewing dump, the normalized reflection noise is given by

$$\frac{n_{vd}}{s(\omega_i, t)} = Q(1 - \eta) \frac{i(\omega_i, t)}{s(\omega_i, t)} \approx Q(1 - \eta) [n_{nc}(\omega_i, t) \leq s(\omega_i, t)], \quad (43)$$

where Q , η , s and i have already been defined, n_{vd} is the "viewing dump noise," and we realize that the dc component of the reflection is filtered out either electronically or digitally.

When the natural linewidth l_{ns} of the ECE in the cross-ing volume of the two sightlines is greater than the correlation length l_c of the emission, some emission at the frequency of the cross-correlation function will not survive the correlation analysis. This noncorrelatable emission normalized to the correlated signal is estimated as

$$\frac{n_{nc}}{s(\omega_i, t)} = \left(1 + \frac{l_{ns}}{l_c}\right) \exp \left[\frac{1}{4} \left(\frac{\omega_i - \omega_0}{\delta\omega_c} \right)^2 \right] - 1, \quad (44)$$

where all quantities have been previously defined.

Since each noise source has been defined above in normalized form, the cross-correlation coefficient can now be obtained from Eq. (24) as

$$\begin{aligned} \rho_{12i} &= (1 + \langle n^2 \rangle / \langle s^2 \rangle)^{-1} \\ &= \left(1 + \frac{\langle n_q^2 \rangle}{\langle s^2 \rangle} + \frac{\langle n_{vd}^2 \rangle}{\langle s^2 \rangle} + \frac{\langle n_{nc}^2 \rangle}{\langle s^2 \rangle} \right)^{-1} \\ &= \left(1 + \left(\frac{n_q}{s} \right)^2 + \left(\frac{n_{vd}}{s} \right)^2 + \left(\frac{n_{nc}}{s} \right)^2 \right)^{-1}, \end{aligned} \quad (45)$$

where the third equality follows since in each case $n = cs$, where c is a constant in time, so that $\langle n^2 \rangle = \langle c^2 s^2 \rangle$ and c^2 can be passed through the $\langle \rangle$ operator.

D. Error analysis

The cross-correlation coefficient ρ_{12i} in each channel is now converted into the estimated error (standard deviation σ_{12i}) of the cross-correlation function $R_{12i}(\omega_i, t)$ using Eq. (15). Figure 3 shows a plot of the cross-correlation function $R_{12}(\omega_i, t)$ vs ω_i , within error bars, obtained using Eq. (36) and Eq. (37). It is assumed that the uncertainty (error) in $R_{12}(\omega_i, t)$ at each ω_i is described by a Gaussian distribution with variance σ_{12i}^2 . A Monte Carlo routine uses the estimated standard deviation σ_{12i} to randomize the predicted cross-correlation function $R_{12}(\omega_i, t)$. A plot of the predicted cross-correlation function $R_{12}(\omega_i, t)$ and a typical set of ran-

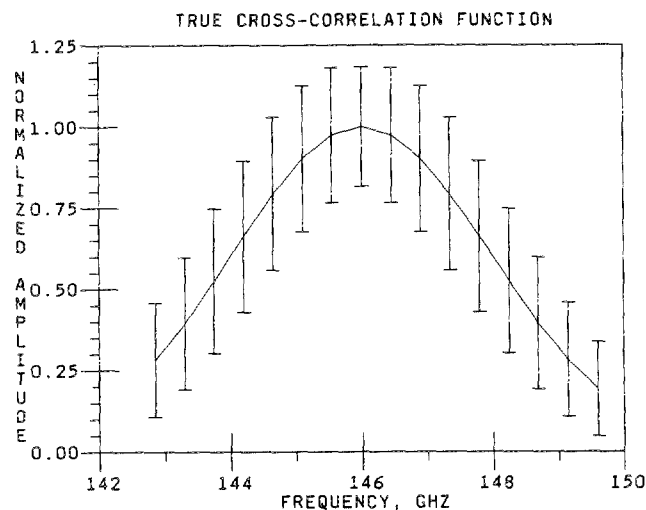


FIG. 3. Typical predicted cross-correlation function vs frequency obtained from the cross-correlation analysis of the ECE emission along the crossed sightlines. The error bars located at the center frequency of each channel show the estimated uncertainty ($\pm 1\sigma$) for this simulation.

domized data are shown in Fig. 4. A nonlinear curve-fitting routine is then used to calculate the line center ω_j of this randomized data. Figure 5 shows a plot of the true cross-correlation function $R_{12}(\omega_i, t)$ and the function fitted to the randomized data. The distance between the line centers of these two functions is the error σ_ω in the line center ω_0 .

The randomization procedure is repeated n times (typically $n = 100$) for each set of plasma parameters. The predicted error in measurement σ_ω of the line center ω_0 is then calculated using

$$\sigma_\omega^2 = \frac{1}{n} \sum_{j=1}^n (\omega_0 - \omega_j)^2 \quad (46)$$

where σ_ω is the standard deviation in the fitted line center,

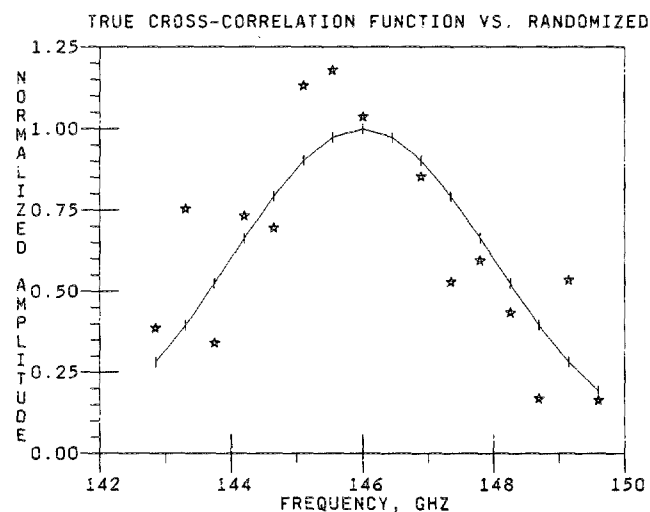


FIG. 4. The predicted cross-correlation function and randomized data vs frequency. The randomized data are obtained using a Monte Carlo routine and the predicted uncertainty in the cross-correlation function.

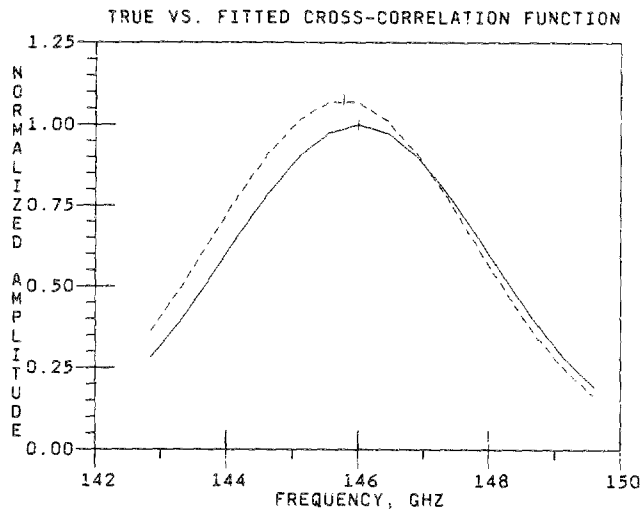


FIG. 5. The predicted cross-correlation function and the function fitted to the randomized data plotted vs frequency. The horizontal separation between the marked line centers is the error in the estimated line center.

ω_0 is the true line center, and ω_j is the line center of the fitted function for the j th set of random data. The standard deviation is divided by the frequency of the true line center ω_0 to obtain the fractional error ϵ_ω in the estimated line center. For each set of plasma parameters, the calculation is repeated for many possible values of A_{f0} , the fractional fluctuation in ECE emission due to fluctuations in density, temperature, or magnetic field.

E. Results

In running this simulation for a particular plasma device, a set of parameters describing the expected conditions for that device must be established. The important param-

eters dependent on the plasma device include the expected relative amplitude of the emission fluctuation compared to the amplitude of the cyclotron peak (the fluctuation fraction A_{f0}), the electron temperature T_e at the crossing volume, the correlation length l_c at the crossing volume, the wall reflectivity R_w , the viewing dump efficiency η , and the integration time T over which the correlation is performed. The parameters which are determined by the diagnostic device design include the number of channels of data per sightline, the bandwidth $\delta\omega_i$, of each channel, the center frequency ω_i of each channel, the response time τ of the microwave crystal detectors, the angle of intersection of the two sightlines, and the digitization rate of the signals at the detectors.

1. TEXT

Figure 6 shows a plot of the fractional error in the magnetic field ($\delta B/B = \sigma_\omega/\omega_0$) vs A_{f0} for the set of reference conditions listed below (see Table I for a description of the parameters listed on Figs. 6–13). Here we assume the amplitude fluctuation A_{f0} (fluctuation fraction) might be due to density fluctuations for instance. The plot shows the error in measuring the line center or absolute value of the magnetic field to be about 1.5×10^{-3} of the field. The absolute magnetic field strength is obtained directly from ω_0 with the same relative error. The time resolution is determined by the averaging time T of the correlation integral. Note that the sawtooth shape of the curves in this plot is due to the statistical nature of the simulation and not to any physical aberration.

In designing our conceptual diagnostic device for TEXT, we have chosen the following parameter values:

- (1) channels per sightline = 16,
- (2) bandwidth of each channel $\delta\omega_i/2\pi = 100$ MHz,
- (3) response time of each microwave crystal detector $\tau = 1 \mu s$,

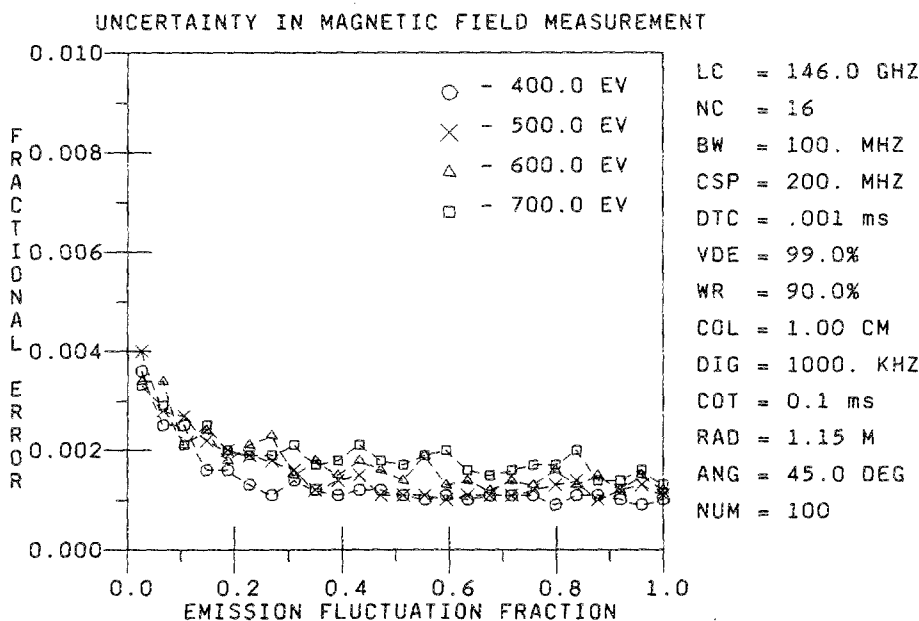


FIG. 6. Uncertainty in the magnetic field measurement for magnetic fluctuations up to 10 kHz on TEXT. The horizontal axis represents the ECE amplitude fluctuation used for correlation (due to n_e fluctuations, for instance). See Table I for a description of the parameter abbreviations on this plot.

TABLE I. Description of parameter list for Figs. 6-13.

LC	The center frequency of the ECE line center at the sightline crossing point, ω_0 .
NC	The number of data channels per sightline.
BW	The frequency bandwidth of each channel, $\delta\omega_i/2\pi$.
CSP	The frequency spacing between channel centers, (channel spacing).
DTC	The response time τ of the microwave crystal detectors (detector time constant).
VDE	The viewing dump efficiency, η .
WR	The vacuum vessel wall reflectivity, R_w .
COL	The assumed correlation length l_c of the plasma fluctuations.
DIG	The digitization frequency of the ADCs.
COT	The correlation time T of the cross correlation integral.
RAD	The sightline crossing point on the major radius, R .
ANG	The angle of intersection of the two sightlines.
NUM	The number of random data sets to be averaged over per set of input parameters.

(4) digitization rate of the detector signals = 1 MHz,
and

(5) angle of intersection of the sightlines = 45° .

For operation on TEXT, we have defined our reference set of parameter values as

- (1) ECE third harmonic line center (2 T operation)
 $\omega_0 = 146$ GHz,
- (2) correlation length $l_c = 1$ cm,
- (3) correlation integration time $T = 100$ μ s,
- (4) wall reflectivity $R_w = 90\%$,
- (5) viewing dump efficiency $\eta = 99\%$, and
- (6) major radius at crossing point, $R = 1.15$ m.

Note that the expected temperature at the crossing volume for TEXT will be between 400 and 500 eV.

The most suspect of the reference conditions is the correlation length l_c . We have estimated l_c in TEXT from Ref. 11. Figure 7 shows that increasing the correlation length by 50% to 1.5 cm causes the relative error to increase from 1.5×10^{-3} to 2.5×10^{-3} . This error can be reduced by vary-

ing other parameters over which we have control. For example in the above case, increasing the correlation integration time by a factor of ten to 1 ms causes the error to drop to 0.5×10^{-3} (see Fig. 8).

For longer correlation times, the error in the measurement of $|B|$ becomes small even for very low fluctuation levels ($A_{f0} \sim 1\%$). Figure 9 shows the expected error for $T = 10$ ms to be less than 0.25×10^{-3} .

Starting with the reference conditions, we performed a sensitivity study on how the error changed with variations in the parameter set. Some general conclusions are that the error decreases when we

- (1) increase the number of channels per sightline and decrease the bandwidth of each channel,
- (2) decrease the response time of the detectors,
- (3) increase the digitization rate (but it cannot be increased above 1 MHz unless the microwave detector time constant τ is decreased and there is true signal at these higher frequencies),

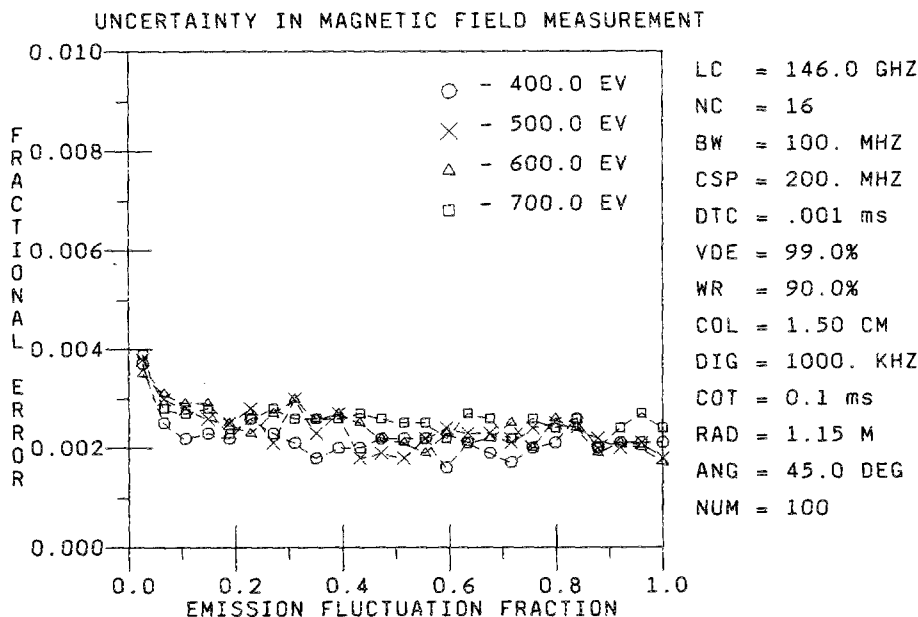


FIG. 7. Same as Fig. 6 for TEXT except that the correlation length has been increased from 1.0 cm to 1.5 cm.

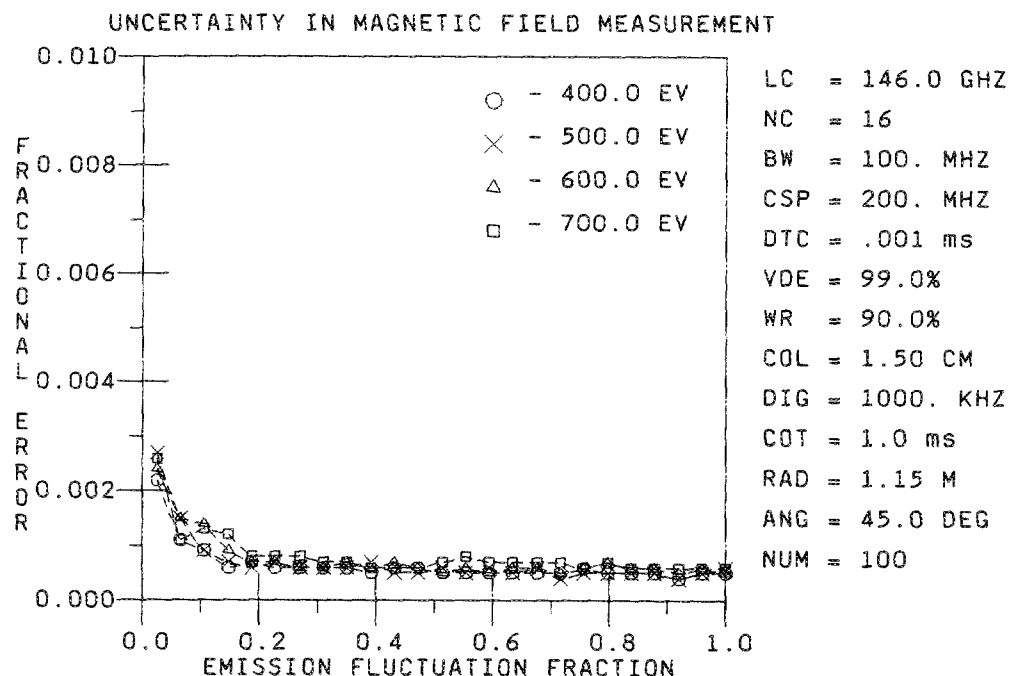


FIG. 8. Same as Fig. 6 except that the correlation length is 1.5 cm as in Fig. 7, and the correlation integration time has been increased to 1 ms so that the frequency response is 1 kHz or less.

- (4) increase the correlation integration time,
- (5) decrease the wall reflectivity, or
- (6) increase the viewing dump efficiency.

The magnitude of the response of the error to changes in the above parameters varies with each parameter, but the error is most sensitive to changes in the digitization rate and correlation integration time.

2. CIT

We have also used our simulation to study the use of this diagnostic on CIT. We believe our results demonstrate that

we can measure $|B|$ in CIT with a resolution of 1×10^{-3} of the toroidal field or better. This can be achieved by correlating the emission in the crossed-sightlines for $T = 10\text{--}100$ ms. This long integration allows the ECE correlation line center ω_0 to be accurately measured even at the very high electron temperatures expected in CIT.

We divided our CIT investigation into two parts, first investigating magnetic fluctuation measurements and then magnetic field ($|B|$) profile measurements. Due to the relativistic spreading of the cyclotron peak as the electron temperature increases, we found that fluctuation measurements at the 1×10^{-3} level with good time resolution will be con-

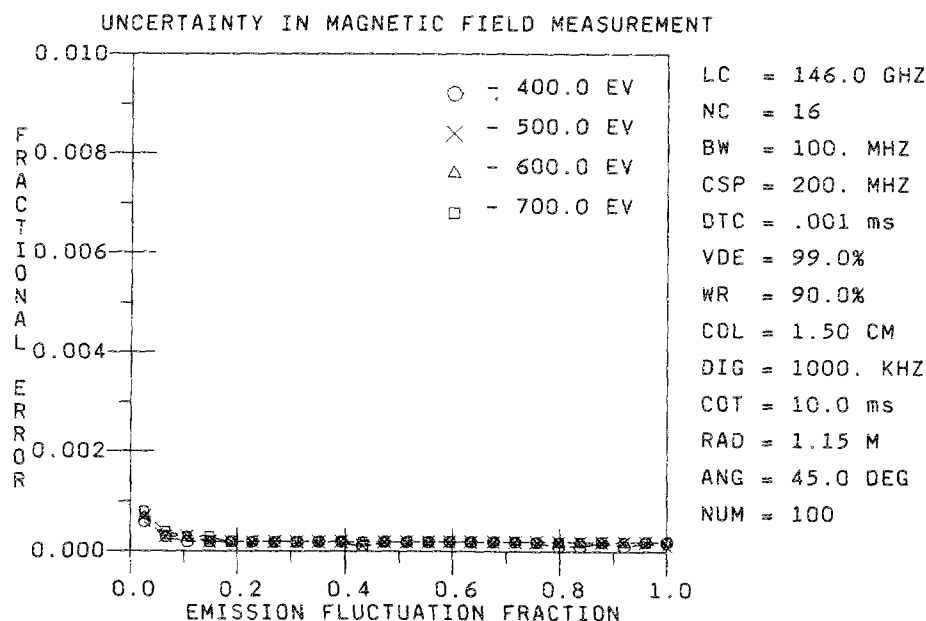


FIG. 9. Same as Fig. 8 except that the correlation integration time has been increased to 10 ms to emphasize the low uncertainty that can be obtained.

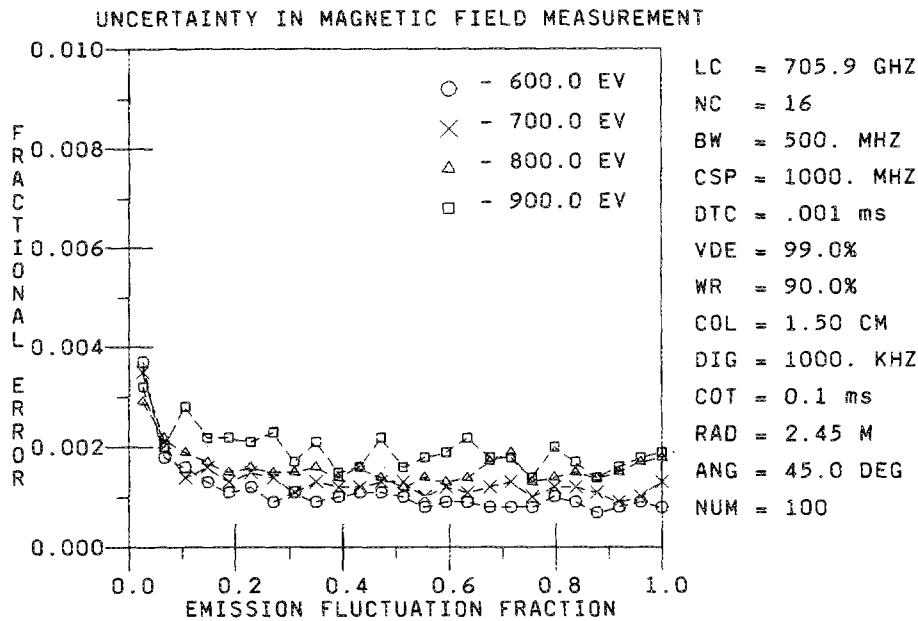


FIG. 10. Uncertainty in the magnetic field measurement on CIT at $r/a = 0.9$ for magnetic fluctuations up to 10 kHz.

finer to the cooler plasma edge region. Figure 10 shows that for the expected conditions in CIT and for our base set of system design parameters we expect to measure parallel fluctuations (if any) in $|B|$ of 1×10^{-3} of the toroidal field at $r/a = 0.9$ and 10 kHz. The parameter set we have defined for CIT to obtain this plot includes $R_0 = 2.0$ m, $a = 0.5$ m, $B_0 = 10.3$ T, $T_{eo} = 10$ keV, and $T_{edge} = 0.5$ keV. These values are not necessarily those given in the latest CIT designs, but they are sufficiently close to the design values to allow for a reasonable simulation of the error in the measurement.

At 10 cm from the edge, the relativistic spreading of the ECE peak begins to greatly increase the error in the mea-

sured line center. The electron temperature increases by almost 1000 eV when moving from $r/a = 0.9$ to $r/a = 0.8$ (for our simulation), and the uncertainty in the $|B|$ measurement increases by a factor of 3. Fortunately, we can vary certain parameters in the data analysis to reduce this uncertainty. In Fig. 11 we have increased the correlation integration time to 10 ms from the 100 μ s in Fig. 10. This increase in the correlation time now allows us to measure $|B|$ to within about 0.25×10^{-3} of the toroidal field but now at 100 Hz. Note that as the natural linewidth of the ECE peak increases, the detector channel bandwidths and channel spacing must also be increased correspondingly.

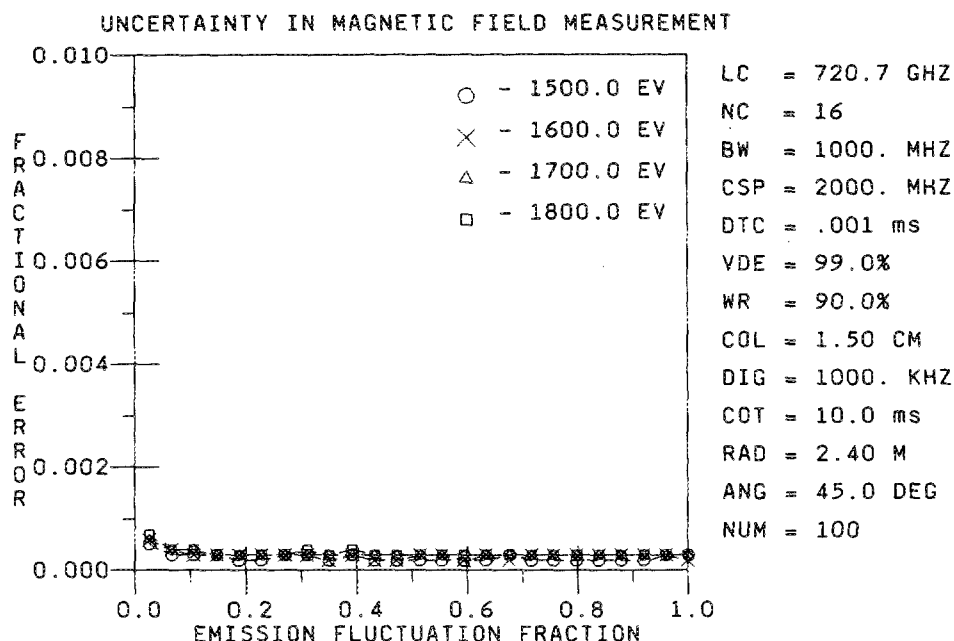


FIG. 11. Same as Fig. 9 for CIT except that the sightline crossing point has been moved to $r/a = 0.8$, and the fluctuation frequency has been decreased to 100 Hz, i.e., correlation integration time of 10 ms.

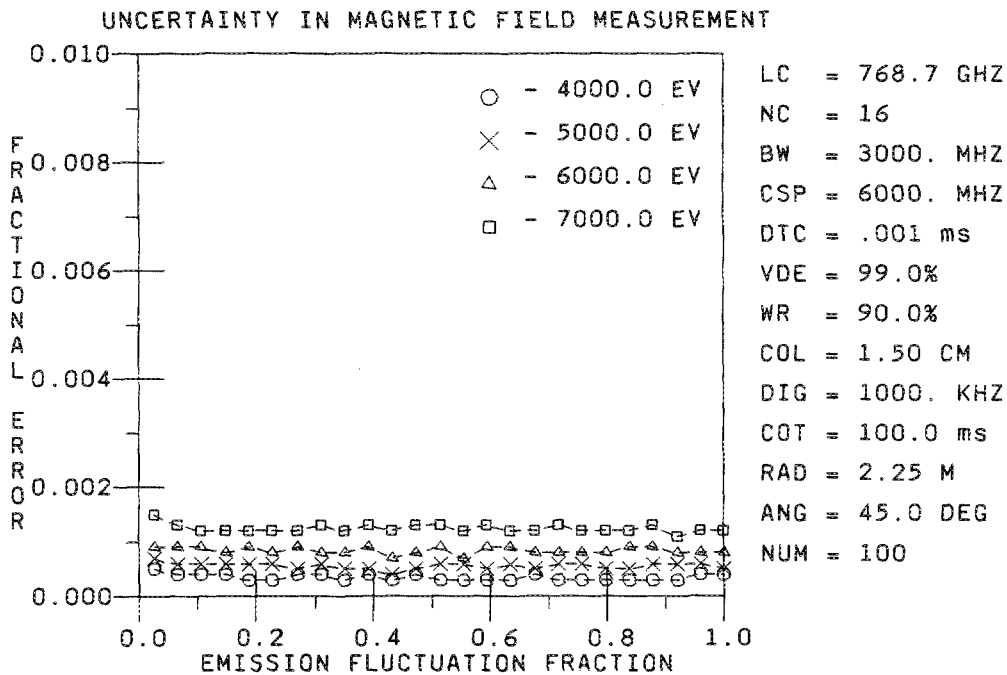


FIG. 12. Uncertainty in the magnetic field measurement on CIT at $r/a = 0.5$ for correlation times of 100 ms.

At $r/a = 0.5$, we take the electron temperature as 5.5–6 keV. Figure 12 shows that at this location with a correlation time of 100 ms, the magnetic field can be measured with an uncertainty of less than 1×10^{-3} of the toroidal field. Figure 13 shows the uncertainty of the magnetic field measurement at the center of the torus, again with a correlation time of 100 ms, to be about 2×10^{-3} of the toroidal field. These two

examples indicate that we can hope to make magnetic field measurements with an error of less than 0.2% (and usually much better) across the CIT plasma. It should also be noted that our diagnostic design has still not been optimized (with regards to picking the number of channels, channel center frequencies, and channel frequency widths) and that optimization may very well increase the resolution.

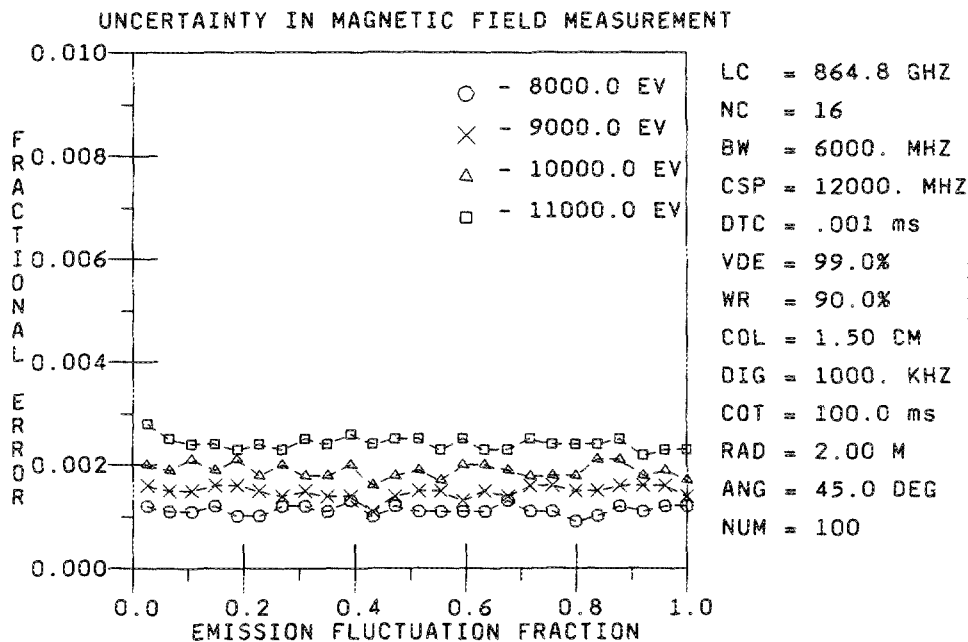


FIG. 13. Same as Fig. 12 for CIT except that the crossing point (measurement point) is now at the plasma center.

VI. NUMERICAL SIMULATION OF THE POLOIDAL MAGNETIC FIELD MEASUREMENT

A. Overview

It was shown in Sec. IV C that the poloidal magnetic field B_θ can be inferred from the $|\mathbf{B}|$ measurement, see Eq. (32). The purpose of this numerical simulation is to determine the uncertainty in inferring B_θ from $|\mathbf{B}|$.

B. Field model

To simulate a B_θ measurement, we begin by assuming a toroidal plasma current profile,

$$j_\phi(r, \theta) = \frac{I_0 [1 - (r/a)^n]}{1 + (r/R_0) \cos \theta}, \quad (47)$$

where I_0 is the normalized (such that the integral gives the total current) central value of the plasma current, r, a, R_0 , and θ are the standard toroidal parameters, and n is a shape factor for the current profile. Then B_θ is calculated by applying Faraday's Law and integrating,

$$B_\theta(r) = \frac{\mu_0}{2\pi r} \int_0^r j_\phi(r, \theta) r dr d\theta. \quad (48)$$

Next an estimate for the toroidal field due to the force-free plasma current $B_{\phi p}$ is obtained from j_θ and the toroidal field $B_\phi \cong B_v + B_d$, where B_v is defined as the standard tokamak vacuum field,

$$B_v = B_0 / (1 + (r/R_0) \cos \theta). \quad (49)$$

B_0 is the central value of the vacuum field, and B_d is obtained from the toroidal equilibrium equation, Eq. (30), as discussed in Sec. IV C. To estimate $B_{\phi p}$ it is assumed that the force free plasma current exactly follows the magnetic field lines so that

$$B_\phi / B_\theta = j_\phi / j_\theta, \quad (50)$$

where j_ϕ is the previously defined toroidal current, and j_θ is the poloidal current. Now solving Eq. (50) for j_θ and substituting in the expressions for j_ϕ , B_ϕ and B_θ , we can write

$$j_\theta(r, \theta) = \frac{\mu_0 I_0^2 [1 - (r/a)^n]}{r B_0 (1 - \beta/2)} \int_0^r \frac{[1 - (r/a)^n]}{1 + (r/R_0) \cos \theta} r dr, \quad (51)$$

where all the above quantities have been previously defined. Using j_θ in Faraday's Law, $B_{\phi p}(r, \theta = 0)$ can be written as

$$B_{\phi p}(r, 0) = \frac{\mu_0}{R_0 + r} \left[\int_0^a (R_0 - r) j_\theta(r, \pi) dr - \int_0^r (R_0 + r) j_\theta(r, 0) dr \right], \quad (52)$$

where it has been assumed that the $|\mathbf{B}|$ measurements will be made on the tokamak midplane with $\theta = 0$. Assuming a profile for beta, $\beta = \beta_0 [1 - (r/a)^m]$, then $|\mathbf{B}|$ is calculated using Eq. (29).

C. Error analysis

Using standard error propagation methods on Eq. (32), the following expression for the uncertainty in the poloidal magnetic field is obtained,

$$\sigma_\theta^2 = \frac{1}{4B_\theta^2} \{ 4|\mathbf{B}|^4 \epsilon_B^2 + 4B_v^2 \epsilon_v^2 \times [B_v(1 - \beta) + B_{\phi p}(1 - \beta/2)]^2 + 4B_{\phi p}^2 \epsilon_{\phi p}^2 [B_{\phi p} + B_v(1 - \beta/2)]^2 + \beta^2 \epsilon_\beta^2 (B_{\phi p} B_v + B_v^2) \}, \quad (53)$$

where $\epsilon_B \equiv \sigma_B / |\mathbf{B}|$ is the uncertainty in the $|\mathbf{B}|$ measurement, $\epsilon_v \equiv \sigma_v / B_v$ is the uncertainty in B_v at the sightline crossing point, $\epsilon_{\phi p} \equiv \sigma_{\phi p} / B_{\phi p}$ is the uncertainty in $B_{\phi p}$, and $\epsilon_\beta \equiv \sigma_\beta / \beta$ is the uncertainty in β . For $B_\theta \ll B_v, \beta \ll 1$, Eq. (53) can be simplified to

$$\epsilon_\theta \equiv \sigma_\theta / B_\theta \cong (|\mathbf{B}| / B_\theta)^2 (\epsilon_B^2 + \epsilon_v^2)^{1/2}. \quad (54)$$

Using the predicted uncertainty in $|\mathbf{B}|$ and assuming reasonable values for the uncertainties in $B_{\phi p}$, B_v , and β , the relative uncertainty ϵ_θ in B_θ can be calculated. Note that for high current or small aspect ratio, Eq. (53) should be used.

D. Results

This simulation calculates the uncertainty in the poloidal magnetic field, inferred from a $|\mathbf{B}|$ measurement, as a function of radius. The required parameters to perform this analysis are the minor radius a , the major radius R_0 , the central magnetic field B_0 , the central beta β_0 , the toroidal plasma current I_T , and the current and beta profile parameters n and m . The estimated uncertainties in $|\mathbf{B}|$, B_v , $B_{\phi p}$, and β are also required.

1. TEXT

Figure 14 shows a plot of the uncertainty in the inferred poloidal magnetic field B_θ versus position along the minor radius for the reference parameter set below for TEXT. This plot indicates that the poloidal magnetic field can be measured with an uncertainty of less than 20% for $r/a \geq 0.2$ and less than 10% for $r/a \geq 0.3$, but for $r/a < 0.2$ the uncertainty increases rapidly as the measurement point moves towards the plasma center. This large uncertainty for $r/a < 0.2$ is due to the small poloidal field near the plasma center. The reference parameter set for this plot is $a = 30$ cm, $R_0 = 1$ m, $B_0 = 1.0$ T, $I_T = 250$ kA, $\beta = 2\%$, $n = 2$, $m = 2$, $\epsilon_B = 0.1\%$, $\epsilon_v = 0.01\%$, $\epsilon_{\phi p} = 0.5\%$, and $\epsilon_\beta = 5\%$.

Starting with this reference parameter set, we performed a sensitivity analysis on each of the parameters. For example, in Fig. 15, B_0 has been increased to 2 T. This causes the uncertainty in B_θ to increase to between 10% and 20% for $r/a \geq 0.4$.

In the $|\mathbf{B}|$ measurement simulation for TEXT, the results given in Sec. V E 1 emphasize faster time resolution; however, if the emphasis is put on reducing the uncertainty in the measurement, then longer correlation times can be used and the uncertainty significantly reduced. For example, if we cut ϵ_B in half to 0.05% (10 ms integration time) then the uncertainty in B_θ is cut in half over the same range. This is shown in Fig. 16.

Examining Eq. (32) and Eq. (54), it can be seen that ϵ_θ decreases as

- (1) the square of the plasma current,

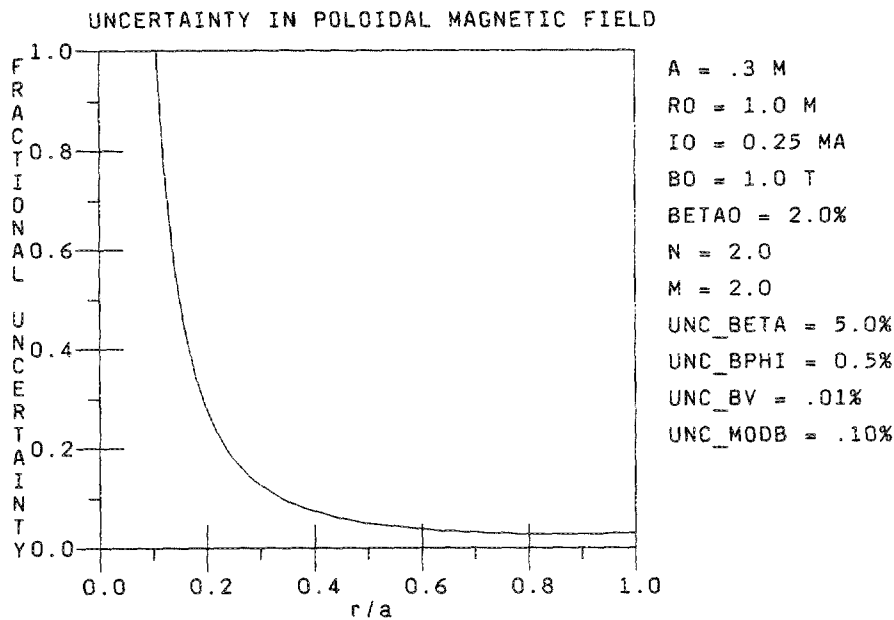


FIG. 14. Estimated uncertainty in the poloidal magnetic field calculated from the $|B|$ measurement on TEXT.

- (2) the square of the decrease in the toroidal magnetic field,
- (3) the current profile parameter n increases,
- (4) the uncertainty in the $|B|$ measurement decreases, and
- (5) the uncertainty in the vacuum field decreases.

Note that β , ϵ_β , and $\epsilon_{\phi p}$ normally have a negligible effect on the uncertainty in B_θ .

2. CIT

For CIT this simulation demonstrates that we can hope to make B_θ measurements for $r/a \geq 0.2$ with an uncertainty of less than 15% and for $r/a \geq 0.4$ with an uncertainty of less than 5%. Figure 17 shows a plot of this uncertainty for the CIT reference parameter set given below. The uncertainty in the B_θ measurement for CIT is much smaller over much of the minor radius than for TEXT because the plasma current,

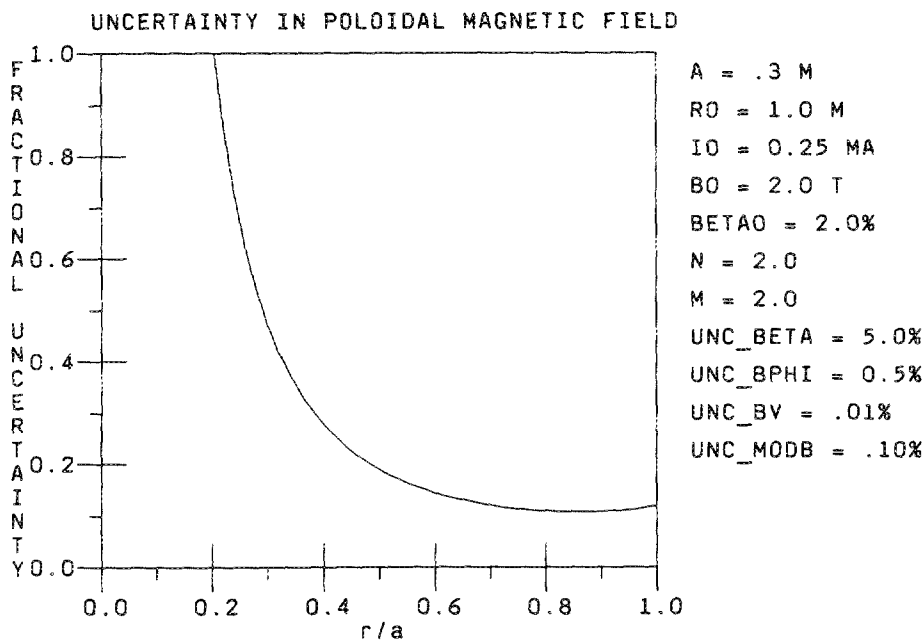


FIG. 15. Same as Fig. 14 except that the magnetic field has been increased to 2.0 T from the 1.0 T in Fig. 14.

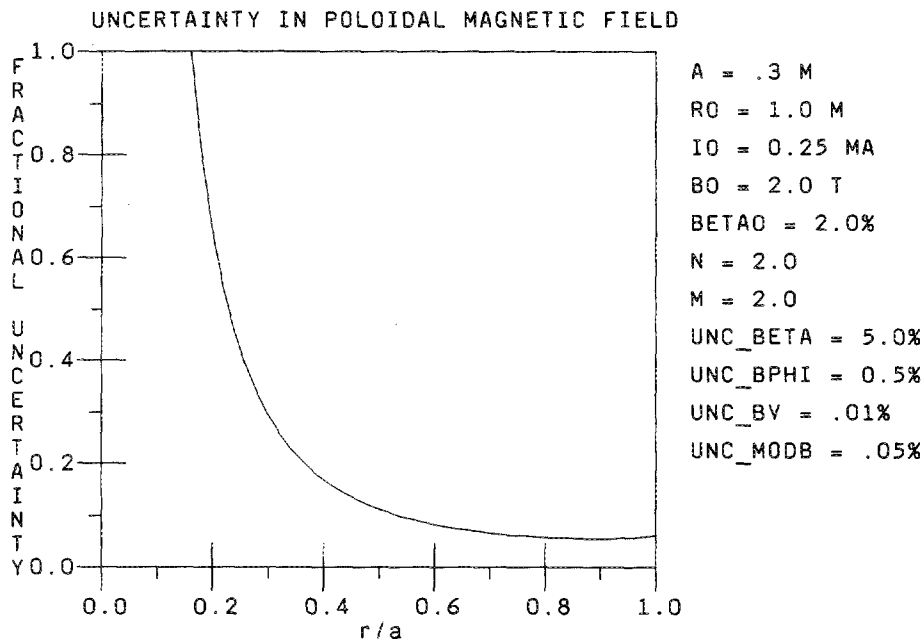


FIG. 16. Same as Fig. 14 except that the magnetic field has been increased to 2 T as in Fig. 15 and the uncertainty in $|B|$ has been decreased to 0.5×10^{-3} .

and therefore B_θ is larger. The reference parameter set for CIT is $a = 0.5 \text{ m}$, $R_0 = 2.0 \text{ m}$, $B_0 = 10.3 \text{ T}$, $I_T = 10 \text{ MA}$, $\beta_0 = 5\%$, $n = 2$, $m = 2$, $\epsilon_B = 0.1\%$, $\epsilon_v = 0.05\%$, $\epsilon_{\phi p} = 5\%$, $\epsilon_\beta = 5\%$.

In Fig. 18, we have reduced B_0 to 7 T and I_T to 7 MA to be more indicative of the initial operating regime expected for CIT. Under these conditions, we can expect to measure B_θ with an uncertainty of less than 10% for $r/a \geq 0.2$.

VII. DISCUSSION

We believe that the calculations above indicate that the potential of this diagnostic is excellent. With careful design and construction, it has a very good chance of measuring parallel fluctuations in $|B|$ as small as 1×10^{-3} of the toroidal field at 10 kHz or even smaller fluctuations at lower frequencies on both TEXT and CIT. Our results also indi-

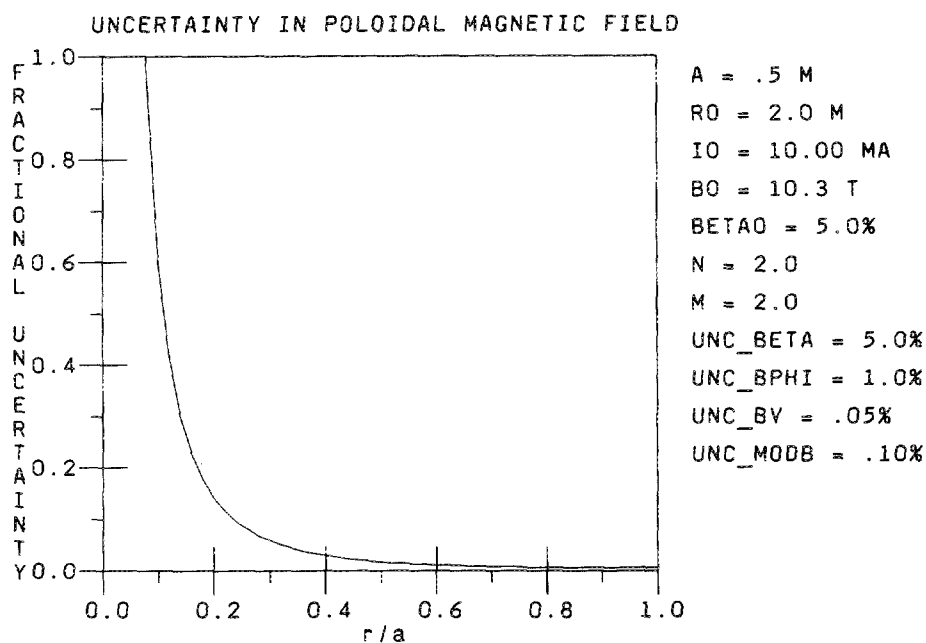
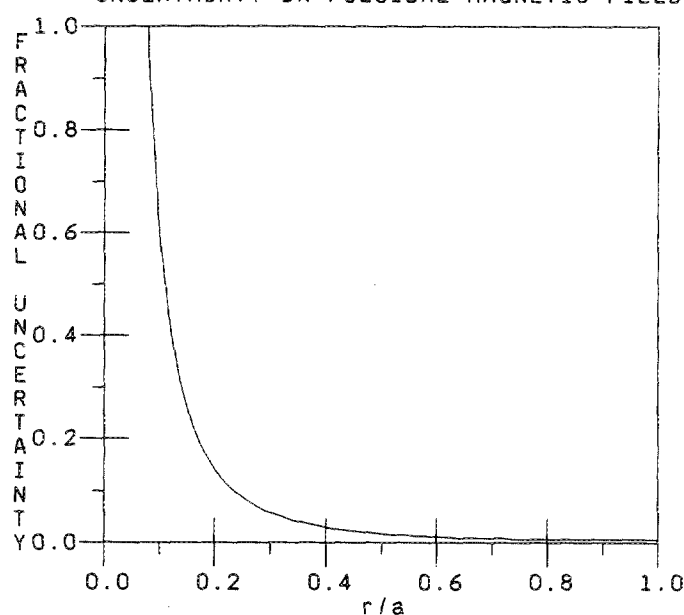


FIG. 17. Estimated uncertainty in the poloidal magnetic field calculated from the $|B|$ measurement on CIT for a high field, high current configuration.

UNCERTAINTY IN POLOIDAL MAGNETIC FIELD



$A = .5 \text{ M}$
 $R_0 = 2.0 \text{ M}$
 $I_0 = 7.00 \text{ MA}$
 $B_0 = 7.0 \text{ T}$
 $BETA_0 = 5.0\%$
 $N = 2.0$
 $M = 2.0$
 $UNC_BETA = 5.0\%$
 $UNC_BPHI = 1.0\%$
 $UNC_BV = .05\%$
 $UNC_MODB = .10\%$

FIG. 18. Uncertainty in the poloidal magnetic field inferred from the $|B|$ measurement on CIT for a low field, low current configuration.

cate that the absolute magnetic field strength can be measured with an uncertainty of less than 0.10% on both devices. With β measurements from another source, we should be able to infer the poloidal magnetic field with an uncertainty of less than 10% for r/a greater than about 0.2. The diagnostic also has the potential of measuring electron temperature and density fluctuations.

ACKNOWLEDGMENTS

Work leading to the conceptual design and numerical simulation of this proposed diagnostic was supported by the United States Department of Energy, Office of Fusion Energy, under contract DE-FG05-87ER53253, and by the Georgia Institute of Technology. We also owe considerable thanks to our colleagues Pete Politzer, John Wilgen, Rex Gandy, Dave Rasmussen, and Jim Callen for useful discussions about this diagnostic.

APPENDIX: DISCUSSION OF COHERENCE OF THE STATISTICAL FLUCTUATIONS OF THERMAL CYCLOTRON EMISSION ON A CROSSED-SIGHTLINE DIAGNOSTIC

It can be shown¹² that the statistical (quantum) fluctuations due to the thermal nature of the electron cyclotron emission (ECE) viewed by two independent detectors looking on crossed sightlines through a plasma are uncorrelated when the two detectors (as seen from the emission volume) are separated by an angle

$$\theta_c = (v_n/2\pi)(\bar{\lambda}/\rho), \quad (55)$$

where v_n is the n th root of the Bessel function $J(v)$, $\bar{\lambda}$ is the center wavelength of the detector bandpass, and ρ is the radius of the ECE source. It has been assumed that the source and detector dimensions are small compared to the distances between them and that the source is a uniform flat disk.

For dimensions typical of the proposed crossed-sight-

line diagnostic ($\bar{\lambda} = 3 \text{ mm}$, $\rho = 1 \text{ cm}$), the angular separation of the two receivers must be 25.9° to assure that the statistical fluctuations in the emission will be uncorrelated. For angles other than 25.9° , the coherence level of the fluctuations to be measured compared to the dc signal must be higher than the coherence level of the statistical fluctuations compared to the dc level. The maximum degree of coherence of the statistical fluctuations for angles greater than 25.9° is 0.14.

In addition to the above, it should also be noted that any coherence of the thermal emission will actually improve the crossed-sightline measurement of the magnetic field (although it would prevent its use for measuring temperature or density fluctuations).

¹ C. E. Thomas Jr., "Using Crossed-Sightline Correlation of Electron Cyclotron Emission to Measure Magnetic Fluctuations in Plasmas", EC6—Joint Workshop on ECE and ECRH, 16–17 Sept. 1987, Oxford, U.K., proceedings.

² C. E. Thomas Jr., G. R. Hanson, R. F. Gandy, D. B. Batchelor, and R. C. Goldfinger, *Rev. Sci. Instrum.* **59**, 1990 (1988).

³ P. R. Bevington, *Data Reduction and Error Analysis for the Physical Sciences* (McGraw-Hill, New York, 1969).

⁴ G. L. Bell, R. F. Gandy, J. B. Wilgen, and D. A. Rasmussen, "ECE Radiation Path Design for ATF", Auburn University Physics Report PR21, Tech. Rep. MMESI-19x-5596V-2, October 1987.

⁵ J. S. Bendat and A. G. Piersol, *Random Data: Analysis and Measurement Procedures*, 2nd ed. (Wiley, New York, 1986).

⁶ Private communication with J. D. Callen, University of Wisconsin, 1988.

⁷ M. Bornatici, R. Cano, O. DeBarbieri, F. Engelmann, *Nucl. Fusion*, **23**, 1153 (1983).

⁸ Private communications with J. B. Wilgen, ORNL, 1988.

⁹ G. Bekefi, *Radiation Processes in Plasmas* (Wiley, New York, 1966), p. 330.

¹⁰ A. Cavallo and R. Cano, *Plasma Phys.* **23**, 65 (1981).

¹¹ D. L. Brower, W. A. Peebles, and N. C. Luhmann, Jr., *Nucl. Fusion*, **27**, 2055 (1987).

¹² M. Born and E. Wolf, *Principles of Optics*, 6th. ed. (Pergamon, New York, 1980).